Cell Mol Neurobiol (2017) 37:1487–1499
DOI 10.1007/s10571-017-0479-z

ORIGINAL RESEARCH

Neurons Internalize Functionalized Micron-Sized Silicon Dioxide Microspheres

Veronica J. Wallace[1] · Raffaello Cimbro[4] · F. Javier Rubio[1] · Lowella V. Fortuno[2] · Julie C. Necarsulmer[2] · Pyry P. Koivula[2] · Mark J. Henderson[2] · Lindsay M. DeBiase[3] · Brandon L. Warren[1] · Brandon K. Harvey[2] · Bruce T. Hope[1]

Received: 2 November 2016 / Accepted: 23 February 2017 / Published online: 4 March 2017

Abstract Microparticles have potential as neuron-specific delivery platforms and devices with many applications in neuroscience, pharmacology, and biomedicine. To date, most literature suggests that neurons are not phagocytic cells capable of internalizing microparticles larger than 0.5 μm. We report that neurons transport fluorescently labeled silica microspheres with diameters of 1–2 μm into neurons in vitro and in rat brain without having overt effects on cell viability. Using flow cytometry, fluorescence-activated cell sorting, and confocal and electron microscopy, we first found that SH-SY5Y human neuroblastoma cells internalized 1-μm silicon microspheres with surface charges of −70 mV (hydroxyl and carboxyl), −30 mV (amino), and +40 mV (ammonio). Uptake was rapid, within 2–4 h, and did not affect cell viability 48 h later. Flow cytometry assays indicate that SH-SY5Y cells internalize 1- and 1.5-μm microspheres at the same rate over a 24-h incubation period. Electron microscopy confirms that SH-SY5Y cells internalize 1-, 1.5-, and 2-μm microspheres. Confocal microscopy demonstrated that primary cortical neurons also internalized 1-, 1.5-, and 2-μm amino microspheres within 4 h. Finally, we injected 1-μm amino microspheres into rat striatum and found microspheres inside neurons. Overall, neurons can internalize microspheres up to 2 μm in diameter with a range of surface chemical groups and charges. These findings allow a host of neuroscience and neuroengineering applications including intracellular microdevices within neurons.

Keywords Silica · Microparticles · Neuroengineering · Brain · Intracellular devices · Phagocytosis · Endocytosis · Internalization

✉ Bruce T. Hope
bhope@intra.nida.nih.gov

[1] Neuronal Ensembles in Addiction Section, Behavioral Neuroscience Research Branch, IRP/NIDA/NIH, 251 Bayview Drive, Baltimore, MD 21224, USA

[2] Optogenetics and Transgenic Technology Core, IRP/NIDA/NIH, 251 Bayview Drive, Baltimore, MD 21224, USA

[3] Synaptic Plasticity Section, Cellular Neurobiology Research Branch, IRP/NIDA/NIH/DHHS, 251 Bayview Blvd, Suite 200, Baltimore, MD 21224, USA

[4] Division of Rheumatology, Bayview Flow Cytometry Core, Johns Hopkins University School of Medicine, Baltimore, MD, USA

Introduction

Microparticles and nanoparticles composed of polymers, hydrogels, and silicon dioxide have been proposed as cell-specific delivery platforms and devices with many applications in neuroscience, pharmacology, and biomedicine (Benoit et al. 2000; Chirra and Desai 2012; Cleland 1999; Skop et al. 2013; Stukel et al. 2015; Varde and Pack 2004; Wang et al. 2014). In vitro studies have shown that nanoparticles can be used to deliver drugs in a cell-specific manner to intracellular targets in a variety of cell types, including neurons and neuron-like cells (Yan et al. 2014). Studies using live animals have used nanoparticles to target neuronal tumor cells, identify known markers of neuronal cancers (Guerrero-Cazares et al. 2014; Kaluzova et al. 2015; Sharpe et al. 2012), and examine neurological disease and damage associated with HIV infection (Avdoshina et al. 2016) and drug addiction (Pilakka-Kanthikeel et al. 2013). Microparticles in the range of 1-μm size could be used to deliver larger payloads (Taylor et al. 2014), allow more options for tracking and imaging particles in vivo (Ebert et al. 2007), and potentially for intracellular

biomedical and bioelectronics devices. Bioelectronic medicine is a growing field with in vivo applications on the micron scale (Simon et al. 2016). In particular, interest has already grown in delivering micron-sized devices into neurons to monitor or manipulate their activity at single-cell resolution (Nakatsuji et al. 2015; Robinson et al. 2012; Vitale et al. 2015). However, little is known about how neurons may internalize micron-sized particles.

Cells, including neurons, use a variety of endocytic mechanisms to internalize extracellular material (Doherty and McMahon 2009; Mukherjee et al. 1997; Sahay et al. 2010). Cells have classically been characterized as phagocytes if they are able to internalize material larger than 0.5 μm, or non-phagocytes if they cannot (Freeman and Grinstein 2014; Rabinovitch 1995). Phagocytic cells use a variety of mechanisms that may also be cell-specific (Aderem and Underhill 1999; Caron and Hall 1998; Lew et al. 1985). Neurons are generally thought to be non-phagocytic and thus unable to internalize particles larger than 0.5 μm (Gordon 2016). However, two previous studies indicate that neurons are capable of internalizing micron-scale particles (Ateh et al. 2011; Bowen et al. 2007).

In the current study, we further examined the ability of neurons to internalize fluorescently labeled micron-sized silica microspheres. Using a variety of techniques, we evaluated uptake of 1-, 1.5-, and 2-μm silica microspheres with different chemical groups and surface charges, including hydroxyl (OH, −70 mV), carboxyl (COOH, −70 mV), amino (NH_2, −30 mV), and ammonio (NH_3, +40 mV) into SH-SY5Y human neuroblastoma cells. We also examined uptake of 1-, 1.5-, and 2-μm microspheres into primary cortical neurons (PCNs) and neurons in the striatum of live rats.

Materials and Methods

Microspheres

All microspheres were obtained from Micromod Partikeltechnologie GmbH; http://www.micromod.de. We used the following microspheres: 1-μm sicastar-redF OH (40-00-103), 1-μm NH_3 sicastar-redF (40-05-103, custom order), 1-μm NH_2 sicastar-redF (40-01-103), 1-μm COOH sicastar-redF (40-02-103), 1.5-μm NH_2 sicastar-redF (40-01-153, custom order), and 2-μm NH_2 sicastar-redF (40-01-203, custom order). Microspheres were synthesized using a silica seed and grown by adding silylated dye, tetraalkoxysilane (TEOS), and aminopropyl-TEOS, resulting in non-porous red fluorescent silica microspheres with maximal excitation at 569 nm and maximal emission at 585 nm, and a polydispersity index of less than 0.2. 1-μm NH_3 sicastar-redF microspheres were synthesized by the same process but with final addition of silyl propyl(octadecyl)dimethyl ammonium chloride to achieve a +40 mV charge at physiological pH. Particle size distribution and charge were characterized using Malvern Instruments Zetasizer ZS90. Each stock solution of microspheres was provided as 50 mg/ml in water.

SH-SY5Y Cell Culture

Based on procedures previously described in (Henderson et al. 2013), SH-SY5Y cells were grown in DMEM with 4.5 g/l glucose and 110 mg/ml sodium pyruvate (Gibco), 10% bovine growth serum (Hyclone), 100 units/ml penicillin, and 100 μg/ml streptomycin (Gibco) in a 37 °C humidified incubator with 5.5% CO_2 prior to any microsphere treatments.

For Flow Cytometry Experiments

SH-SY5Y cells (passages 17–31) were plated at 5×10^5 viable cells per well on untreated flat bottom 6-well plates and grown 24–48 h prior to microsphere treatments. Microspheres were diluted from the stock solution into pre-warmed Opti-MEM minimal media (Gibco) and vortexed at high speed for approximately 30 s immediately before adding 2 ml of the diluted microsphere solution to the cells using a complete media exchange. For microsphere concentration experiments, the final dilutions were 0.2, 2, 20, and 200 μg/ml (corresponding to 1.9×10^5, 1.9×10^6, 1.9×10^7, and 1.9×10^8 microspheres/ml, respectively). Plates were immediately returned to the incubator at 37 °C for 3 h. For time course experiments, the final dilution was 5 μg/ml or 4.75×10^6 microspheres/ml. According to final cell counts conducted after microsphere treatment, a concentration of 5 μg/ml corresponded to a ratio of approximately five microspheres per cell. Plates were immediately returned to 37 °C for 0–24 h of incubation. Following incubation, non-cell-associated microspheres were removed by aspiration and cells were washed three times with 2 ml of 1× PBS. For 0-h time points, the microsphere solution was added to the cells and washed immediately with 1× PBS. Cells from each well were then trypsinized, harvested, and processed for flow cytometry.

For Experiments with Fluorescence-Activated Cell Sorting (FACS)

SH-SY5Y cells (passages 15–30) were plated at 5×10^5 viable cells per well on untreated flat bottom 6-well plates and grown for 48 h prior to microsphere treatments. Microspheres were diluted from the stock solution to 20 μg/ml in pre-warmed Opti-MEM minimal media and

vortexed at high speed for approximately 30 s immediately before adding 2 ml of microsphere solution to the cells using a complete media exchange. Plates were immediately returned to 37 °C for 3 h prior to processing for FACS.

For Electron Microscopy Experiments

SH-SY5Y cells (passage 23) were plated at 5×10^5 viable cells per well on untreated flat bottom 6-well plates and grown for 48 h prior to microsphere treatments. Microspheres were diluted from the stock solution to 20 μg/ml in pre-warmed Opti-MEM minimal media and vortexed at high speed for approximately 30 s immediately before adding 2 ml of microsphere solution to the cells using a complete media exchange. Plates were immediately returned to 37 °C for 4 h prior to processing for electron microscopy.

Primary Cortical Neuron (PCN) Culture

Rat primary cortical neurons (PCNs) were harvested and maintained as described previously in (Howard et al. 2008). Cells were plated at 2×10^5 viable cells per well on PEI-coated glass coverslips in untreated flat bottom 24-well plates using Neurobasal media (Invitrogen), 2% heat-inactivated fetal bovine serum (Sigma-Aldrich, Milwaukee, WI), 2% B27 supplement (Invitrogen), 0.5 mM L-glutamine, and 0.025 mM L-glutamate in a 37 °C humidified incubator with 5.5% CO_2. Cells were maintained with feeding media consisting of Neurobasal media, 2% B27 supplement, and 0.5 mM L-glutamine for 14 days prior to microsphere treatment. Microspheres were introduced to cells by 50% media exchange: half of the cell culture media (500 μl) was replaced with 500 μl of 10 μg/ml microspheres in fresh PCN feeding media for a final microsphere concentration of 5 μg/ml. Plates were immediately returned to 37 °C for 4 or 8 h prior to processing for confocal microscopy.

Flow Cytometry

Following incubation with microspheres, SH-SY5Y cells were washed thoroughly with sterile 1× PBS and lifted from the plates using 0.05% trypsin–EDTA. Harvested cells were collected in 15 ml conical tubes (Falcon/Corning) and centrifuged for 5 min at 1000 RPM. Supernatant was removed by aspiration, and the cell pellet was resuspended in 350 μl 1× PBS. In microsphere concentration experiments, cells remained unlabeled. In time course experiments, dead cells were labeled with LIVE/DEAD fixable far-red dead cell stain kit (ThermoFisher Scientific) according to the manufacturer's recommended protocol. For both types of experiments, small portions of samples were labeled with 10 μg/ml of DAPI (4′,6-diamidino-2-phenylindole, dihydrochloride) initially to set the flow cytometer gates. All cell samples were filtered through 40 μm filter tops into flow cytometry sample tubes (Falcon/Corning). All cells were run unfixed at low flow speed in a BD FACS Canto II flow cytometer, and at least 10,000 cell events were recorded from each sample. FACS Diva software was used to acquire and analyze the results.

Fluorescence-Activated Cell Sorting

Following incubation with microspheres, cells were washed with 1× PBS and lifted from the plates using 0.05% trypsin–EDTA. Briefly, cells were fixed in 4% PFA for 15 min in 1.5 ml Lo-bind Eppendorf tubes using end-over-end mixing at 22 °C. After washing in 1× PBS, cell nuclei and membranes were labeled simultaneously with 1 μl of 10 mg/ml DAPI and 10 μl of 1 mg/ml wheat germ agglutinin (WGA) conjugated to Alexa Fluor-647 (AF647) in 1 ml of 1X PBS in Lo-bind Eppendorf tubes for 10 min using end-over-end mixing at 22 °C. Cells were washed again and placed on ice. The cells were sorted at the Johns Hopkins Bayview Flow Cytometry Core Facility using a BD FACS Aria I Special Order cell sorter. Cells were collected in 1× PBS in Lo-bind 1.5 ml Eppendorf tube. After sorting, cells were mounted onto microscope slides by drop-wise pipetting into Mowiol mounting media and coverslipped for epifluorescent microscopy. Images were captured with a QImaging Rolera em-c^2 camera attached to a Nikon Eclipse E800 microscope and 60× oil immersion objective.

Transmission Electron Microscopy (TEM)

Following incubation with microspheres, cells were washed thoroughly with 1× PBS. Each well of cells was fixed overnight at 4 °C in 5 ml of 2.5% EM grade glutaraldehyde and 3 mM $MgCl_2$ in 0.1 M sodium cacodylate buffer (pH 7.2). Cells in plates were transported to the Johns Hopkins University School of Medicine Institute for Basic Biomedical Sciences Microscope Facility and fixed a second time in the same fixative for 1 h at 22 °C. After washing, samples were post-fixed in 1% osmium tetroxide and 0.8% potassium ferrocyanide in 0.1 M sodium cacodylate buffer for 1 h on ice in the dark. After washing the cells with distilled water, the plates were stained with 2% aqueous uranyl acetate for 1 h in the dark, dehydrated in a graded series of ethanol, and embedded in Eponate 12 (Ted Pella) resin. Samples were polymerized at 37 °C for 2–3 days before incubation at 60 °C overnight. Thin sections (60–90 nm) were cut with a diamond knife on a Reichert-Jung Ultracut E ultramicrotome and picked up with 2 × 1 mm formvar-coated copper slot grids. Grids

were stained with 2% uranyl acetate in 50% methanol and 0.4% lead citrate before imaging on a Philips CM120 at 80 kV. Images were captured with an AMT XR80 CCD (8 megapixel) camera.

Confocal Microscopy of PCNs

Following incubation with microspheres, the cells on coverslips were washed with 1× PBS and fixed with 4% PFA for 40 min at 22 °C. Cell membranes were labeled with 10 µl of 1 mg/ml WGA conjugated with Alexa Fluor 647 in 1 ml of 1× PBS per well in 24-well plate for 10 min at 22 °C. Cell nuclei were subsequently labeled with 1:1000 solution DAPI (10 µg/ml) in 1× PBS for 10 min at 22 °C. Cells were then washed and mounted onto microscope slides with Mowiol mounting media. Stacks of confocal images of the cells were acquired using a 60× oil immersion objective and Olympus FV 1000 laser scanning microscope (Olympus Corporation of the Americas, Waltham, MA), 1.5× digital zoom and 0.2 µm z-interval. Acquired images were deconvolved separately with Huygens Essential X11 software and then imported into Image J image analysis software. Microsphere internalization was determined through analysis of fluorescence colocalization in the XY and orthogonal XZ, YZ projections of images stacks. Cells with microspheres (3–5 cells per well) were randomly selected for analysis.

Microsphere Injections into Brain

Nine adult Long Evans rats (Charles River) that weighed 275–500 g at the time of surgery were used for this study. After surgery, rats were housed individually under a reverse 12-h light–dark cycle (lights off at 8:00 AM). Food and water were freely available in the rats' home cages throughout the experiment. All procedures were approved by the NIDA IACUC and followed the guidelines outlined in the *Guide for the care and use of laboratory animals* (Ed 8; http://grants.nih.gov/grants/olaw/Guide-for-the-Care-and-Use-of-Laboratory-Animals.pdf). Rats were anesthetized with isoflurane followed by intraperitoneal injections of 80 mg/kg ketamine + 8 mg/kg xylazine dissolved in 0.9% sterile saline to maintain anesthesia. Using a stereotaxic apparatus (Stoelting Company), rats were injected bilaterally with microspheres in sterile 1× PBS at a concentration of 5, 50, and 500 µg/ml (corresponding to 4.75×10^6, 4.75×10^7, and 4.75×10^8 microspheres/ml, respectively) into the striatum using stereotaxic coordinates (anteroposterior 0.0 relative to Bregma, mediolateral ± 3.0). One microliter was injected as the needle was moved slowly from −6.8 to −5.8 dorsoventrally. One minute after injection of the first microliter completed, the needle was raised and a second microliter was injected between −4.8 and −3.8, for a total of 2.0 µl microspheres delivered to each striatal hemisphere. Two minutes after completion of the second injection, the needle was slowly removed from the brain. Rats were allowed to recover for 24 h.

Rats were then deeply anesthetized using isoflurane for 90 s and transcardially perfused with 100 ml of 1× phosphate-buffered saline (PBS), followed by 400 ml of 4% paraformaldehyde (PFA) in 0.1 M PBS. Rat brains were then post-fixed for 90 min in paraformaldehyde followed by cryopreservation in 30% sucrose in 1× PBS at 4 °C for 2–3 days. Brains were then frozen in powdered dry ice and kept at −80 °C until sectioning. Coronal sections (40 µm) were labeled with 1:500 dilution of 640/660 Neurotrace Nissl stain (ThermoFisher Scientific, 640 max excitation, 660 max emission) for 20 min at 22 °C using the manufacturer's recommended protocol for labeling brain cryosections and then labeled with 1:2000 dilution of DAPI (5 µg/ml) in 1× PBS for 15 min at 22 °C to label nuclei. Tissue sections were washed thoroughly with 1× PBS, mounted on to microscope slides, and coverslipped with Mowiol mounting media. High magnification Z-stacks of confocal images were acquired using a 60× oil immersion objective and Olympus FV 1000 laser scanning microscope (Olympus Corporation of the Americas, Waltham, MA), 1.5× digital zoom and 0.2 µm z-interval. Acquired images were deconvolved separately with Huygens Essential X11 software and then imported into Image J image analysis software. Low magnification Z-stack images to assess field of view for multiple neurons were obtained using 20× air or 60× oil immersion objective without zoom and 0.3 µm z-interval on the same microscope. Maximum intensity projections of z-stacks were constructed using Image J.

Statistics

All experiments using flow cytometry were conducted independently three times. Statistical analyses were performed by two-way ANOVA using Prism (Graphpad Software). Dunnett's test was used for post hoc analyses when prior ANOVAs indicated significant main or interaction effects ($p < 0.05$).

Results

We first assessed internalization of red fluorescent silica microspheres functionalized with different chemical groups and surface charges into SH-SY5Y cells, a human neuroblastoma cell line. Plated cells were incubated for 3 h with or without the addition of 1-µm microspheres (Fig. 1a, b). Following enzymatic and mechanical dissociation into single cells (Fig. 1c, d), we used flow cytometry to assess

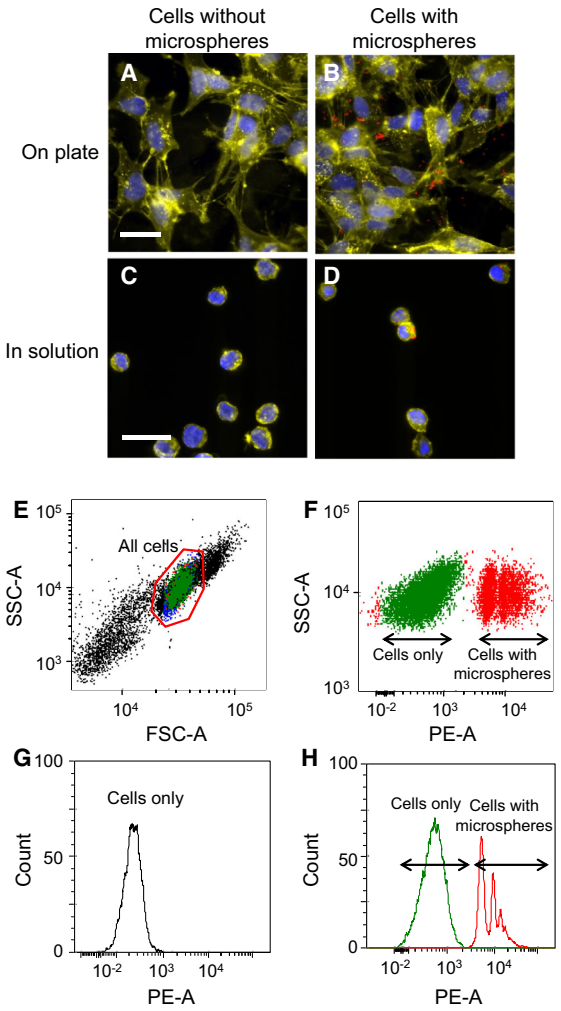

Fig. 1 Using flow cytometry to assess internalization of microspheres into SH-SY5Y neuroblastoma cells. **a**, **b** SH-SY5Y neuroblastoma cells were incubated for 4 h with and without 5 µg/ml 1-µm amino (NH_2, −30 mV) red fluorescent silica microspheres. Cell nuclei were labeled with DAPI (*blue*) and the cell membranes were labeled with wheat germ agglutinin conjugated to Alexa Fluor 647 (*yellow*). **c**, **d** Following a 4-h incubation with 5 µg/ml amino (NH_2, −30 mV) 1-µm microspheres, SH-SY5Y cells were lifted from the plate and suspended in 1× PBS solution. *Scale bar* indicates 40 µm. Cells in solution were then analyzed in a flow cytometer. **e** A cluster of events (inside the red gate) within a forward and side scatter dot plot were identified as 'Cells' by DAPI-labeling and gated for further analysis. **f** Cells gated in the forward-side scatter plot were then assessed for red fluorescence (PE) from the microspheres. Isolated cells analyzed with flow cytometry showed distinct cell populations at a range of PE values corresponding to the number of microspheres associated with each cell. Histograms (**g**, **h**) indicate the number of cells (*y*-axis) with different levels of red fluorescence (*x*-axis) in the dot plots in panels (**e**, **f**). The large peak with low PE fluorescence in histograms (**g**, **h**) corresponds to cells without microspheres, while the peaks with higher levels of PE fluorescence in histogram (**h**) correspond to cells associated with one or more red fluorescent microspheres

the association between the cells and the red fluorescent microspheres. Cells and microspheres were detected in the PE (phycoerythrin) channel on the flow cytometer. For illustration purposes only, a subset of cells was fixed, the membranes labeled with WGA-Alexa Fluor 647 and the nuclei labeled with DAPI, prior to epifluorescence imaging (Fig. 1a–d). All remaining experiments using flow cytometry were performed using unfixed and unlabeled cells. The scatterplot in Fig. 1e indicates forward scatter (particle size) and side scatter (granularity or cell complexity) characteristics of all particles or events (dots in plot) in the sample. Small samples of DAPI-labeled cells were used to properly identify and gate cells for subsequent samples (Fig. 1e "All Cells" gate). In Fig. 1f, we show PE fluorescence intensity, indicating the presence of silica microspheres associated with the SH-SY5Y neuroblastoma cells. Cells with PE fluorescence below the relative intensity of 10^3 units (Fig. 1f; green dots) did not contain microspheres, while cells with PE fluorescence above 10^3 units (red dots) contain one or more microspheres. The histograms in Fig. 1g, h quantify the number of events at each level of PE fluorescence from the scatterplots. As an example, the histogram in Fig. 1h quantifies events from the scatterplot Fig. 1f. In cell samples incubated with microspheres, we noted discrete peaks with increasing levels of PE fluorescence that may represent cells containing different numbers of microspheres per cell (Fig. 1h). In cell samples without microspheres, we confirmed that the cluster of events with PE fluorescence below 10^3 units (indicated as 'Cells only') identify cells that are not associated with microspheres (Fig. 1g).

To confirm that flow cytometry could be used to quantify the number of microspheres per cell, we sorted cells from the individual PE fluorescent peaks 1, 2, 3, 4 into separate collection tubes and assessed the number of microspheres per cell using epifluorescence microscopy (Fig. 2b). One hundred cells from each peak were analyzed using epifluorescence microscopy to assess the mean ± SEM number of red fluorescent microspheres associated with each cell; four examples of cells from each peak are shown in Fig. 2b. Peaks 1, 2, 3, and 4 contained 1.02 ± 0.06, 1.73 ± 0.07, 2.92 ± 0.14, and 6.28 ± 0.34 microspheres per cell, respectively. None of the 100 cells examined from the 'Cells only' peak contained red fluorescent microspheres. These data indicate that peaks 1, 2, 3, and 4 in these flow cytometry assays contained cells with approximately 1, 2, 3, and 4+ (4 or more) microspheres associated with each cell.

Using only flow cytometry, we cannot completely exclude that the PE fluorescent microspheres in the above experiments are adsorbed to the outside of the SH-SY5Y cells rather than being internalized. To confirm that these microspheres can be internalized in these cells, we incubated the cells with 1-, 1.5-, or 2-µm microspheres (NH_2 chemistry with surface charges of −30 mV, −38 mV, and −22 mV respectively) using the same process as above and

examined their cellular location using electron microscopy. It was not possible to manufacture differently sized microspheres made in different lots with exactly the same surface charges. Internalized microspheres could clearly be observed in randomly selected cells (Fig. 3). Many of these cells, but not all, had 1-, 1.5-, and 2-μm-size microspheres inside them. These microspheres appeared to be in the cytoplasm and not associated with any membranous organelles. Overall, the evidence from epifluorescence and electron microscopy, as well as washing and trypsinization to remove extracellular absorbed microspheres in the flow cytometry samples, indicate that the histogram peaks in the flow cytometry results are due to internalization of microspheres into the cells.

We then used the peak information from the flow cytometry assay to evaluate uptake of 1-μm microspheres with different surface chemistries and surface charges, including COOH (−70 mV), OH (−70 mV), NH_2 (−30 mV), and NH_3 (+40 mV) into SH-SY5Y cells. Incubating the cells with increasing concentrations (0.2–200 μg/ml) of each microsphere surface type increased the percentage of cells that contained one or more microspheres (Fig. 4a). Two-way ANOVA indicates main effects of Surface type ($F_{3,32} = 35.3$, $p < 0.0001$) and Concentration ($F_{3,32} = 540.9$, $p < 0.0001$), and a significant interaction ($F_{9,32} = 6.6$, $p < 0.0001$). Separate post hoc analyses (Dunnett's test) for each microsphere surface type indicate that 2, 20, and 200 μg/ml of all microsphere surface types significantly increased the percentage of cells containing microspheres, relative to values from the 0.2 μg/ml group, with the one exception of 2 μg/

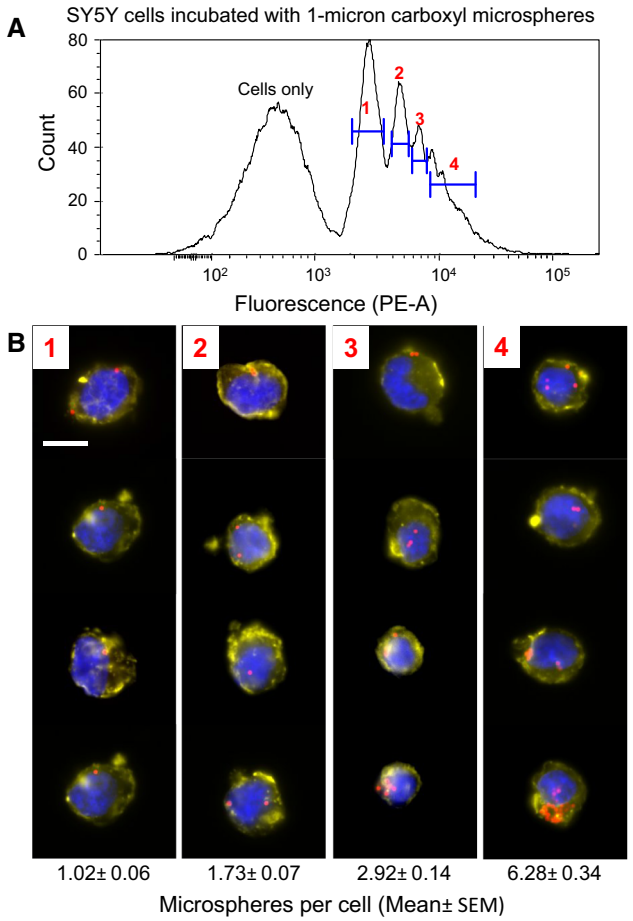

Fig. 2 PE fluorescence in flow cytometry corresponds with number of red fluorescent microspheres in each cell. SH-SY5Y cells were incubated with 20 μg/ml of 1-μm carboxyl microspheres (COOH, −70 mV) for 3 h and then FACS-sorted based on their PE fluorescence (*x*-axis). **a** Low-fluorescence peaks were separated from the high-fluorescence peaks that were numbered 1–4 in the flow cytometry histogram. **b** FACS-sorted cells from each of peaks 1–4 ($n = 100$ cells per peak) were collected and the numbers of particles per cell were counted using epifluorescent microscopy. *Scale bar* indicates 10 μm. The number of red microspheres per cell (mean ± SEM) for each of the peaks 1–4 is indicated below each row of images. The 'Cells only' population was determined in previous experiments. Higher PE fluorescence for peaks 1–4 in the histogram corresponded with higher numbers of red microspheres per cell

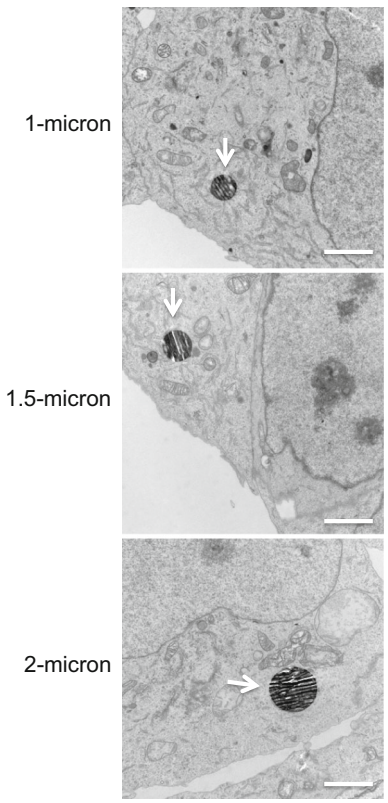

Fig. 3 Electron microscopy confirms internalization of 1-, 1.5-, and 2-μm microspheres into SH-SY5Y cells. SH-SY5Y cells were incubated for 4 h with 5 μg/ml of NH_2-functionalized 1-, 1.5-, or 2-μm microspheres with surface charges of −30 mV, −38 mV, and −22 mV, respectively, and prepared for electron microscopy. Images were captured at 7400× magnification. Images show 1-, 1.5-, and 2-μm microspheres (indicated with *white arrows*) located inside the cell. Note that microspheres appear to be in the cytoplasm and not in any membranous vesicle. *Scale bar* indicates 2 μm

ml of the NH_2 (−30 mV) surface type. All microsphere surface types were significantly different from each other, with the exception of the OH (−70 mV) and COOH (−70 mV) surface types.

The percentage of cells with microspheres increased with incubation time when incubating 5 μg/ml of each microsphere surface type (Fig. 4b). Two-way ANOVA indicates main effects of microsphere Surface type ($F_{3,48} = 13.7$, $p < 0.0001$) and Time ($F_{5,48} = 105.8$, $p < 0.0001$), and a significant interaction ($F_{15,48} = 2.3$, $p = 0.013$). Separate post hoc analyses (Dunnett's test) for each microsphere surface type indicate that the percentage of cells with microspheres was increased at 4, 8, and 24 h, relative to the 0-h time point. The 1-h time point for COOH (−70 mV) microspheres was also increased relative to its 0-h time point. Overall, the OH (−70 mV) and NH_2 (−30 mV) microsphere surface types had similar rates of uptake, but significantly lower than uptake rates for COOH (−70 mV) and NH_3 (+40 mV) surface types. Most of the microsphere uptake had occurred within 8 h and remained stable for up to 24 h. It should be noted that to obtain the 0-h time point, the microspheres were in contact with cells for approximately 5 s and then washed away; thus the values for the 0-h time point includes small numbers of cells non-specifically associated with microspheres during this short time interaction.

We examined whether incubation of cells with microspheres altered cell viability using the LIVE/DEAD® Fixable Far-Red Dead Cell Stain kit and flow cytometry. Incubation of cells with microspheres did not significantly affect cell viability (Fig. 4c). Two-way ANOVA indicates a main effect of Time ($F_{5,53} = 3.8$, $p = 0.0054$) but not for Microspheres ($F_{4,53} = 1.4$, $p = 0.24$), and no interaction ($F_{20,53} = 0.74$, $p = 0.76$). However, post hoc analyses (Dunnett's test) indicate no change in cell viability over time, relative to the 0-h time point.

To understand if the uptake of beads from the cells is a sequential process of one bead at a time or if multiple beads enter the cell at the same time, we separated the microsphere time course data from Fig. 4b into the percentage of cells containing 1, 2, 3, or 4+ microspheres per cell for each microsphere surface type (Fig. 5). For the OH (−70 mV) surface type, two-way ANOVA indicates main effects of Microspheres per cell ($F_{3,48} = 202$, $p < 0.0001$) and Time ($F_{5,48} = 117$, $p < 0.0001$), and a significant interaction ($F_{15,48} = 12.2$, $p < 0.0001$). Separate post hoc analyses (Dunnett's test) for each peak indicate that the percentage of cells containing 1 microsphere was increased at 1, 2, 4, 8, 24 h; 2 microspheres was increased at 4, 8, 24 h; 3 microspheres was increased at 8 and 24 h; 4+ microspheres was increased at 8 and 24 h (relative to the 0-h time point). For the COOH (−70 mV) surface type, two-way ANOVA indicates main effects of Microspheres per cell ($F_{3,48} = 304$, $p < 0.0001$) and Time ($F_{5,48} = 206$, $p < 0.0001$), and a significant interaction ($F_{15,48} = 27$, $p < 0.0001$). Separate post hoc analyses (Dunnett's test) for each peak indicate that the percentage of cells

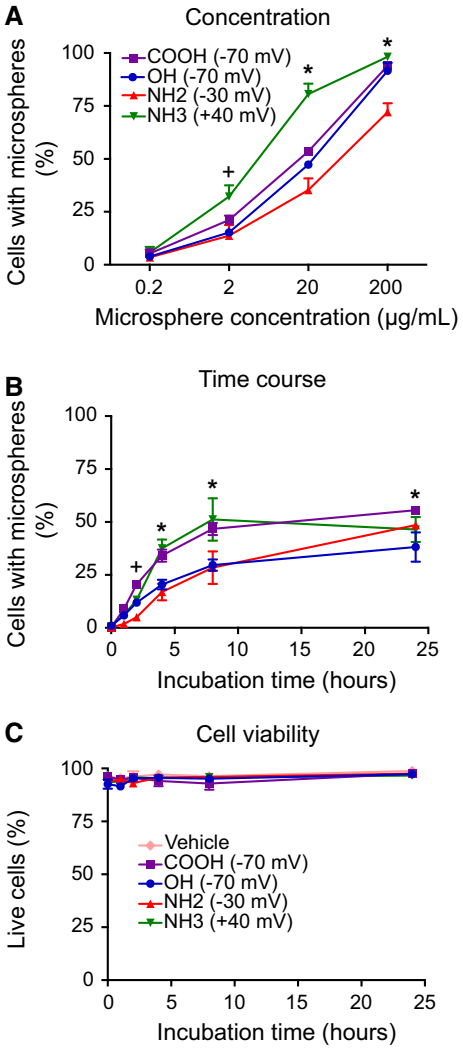

Fig. 4 Concentration, time course, and cell viability for internalization of 1-μm microspheres. **a** SH-SY5Y cells were incubated for 3 h with 0.2–200 μg/ml of 1-μm microspheres with four different surface types (surface charges): carboxyl (COOH, −70 mV), hydroxyl (OH, −70 mV), amino (NH_2, −30 mV), ammonio (NH_3, +40 mV), and microsphere internalization was assessed using flow cytometry. Higher microsphere concentrations led to increasing percentages of cells with microspheres for all surface types and charges. Data are shown as mean ± SEM, $n = 3$, *asterisk* indicates significantly different from 0.2 μg/ml for each surface type, *plus symbol* indicates only COOH and NH_3 are significantly different from their 0.2 μg/ml value. **b** SH-SY5Y cells were incubated for 0–24 h with 5 μg/ml of the four different types of 1-μm microspheres. The cells internalized all microsphere surface types within 2–4 h of incubation. Data are shown as mean ± SEM, $n = 3$, *asterisk* indicates significantly different from 0-h time point for all surface types, *plus symbol* indicates only COOH and NH_3 are significantly different from their 0-h values. **c** Incubation of cells with the microspheres had no effect on cell viability over 24 h. Data are shown as mean ± SEM, $n = 3$

containing 1 microsphere was increased at 1, 2, 4, 8, 24 h; 2 microspheres was increased at 2, 4, 8, 24 h; 3 microspheres was increased at 4, 8, 24 h; 4+ microspheres was increased at 4, 8, 24 h (relative to the 0-h time point). For the NH_2 (−30 mV) surface type, two-way ANOVA indicates main effects of Microspheres per cell ($F_{3,48} = 28$, $p < 0.0001$) and Time ($F_{5,48} = 76$, $p < 0.0001$), and a significant interaction ($F_{15,\ 48} = 3.9$, $p = 0.0002$). Separate post hoc analyses (Dunnett's test) for each peak indicate that the percentage of cells containing 1 microsphere was increased at 4, 8, 24 h; 2 microspheres was increased at 4, 8, 24 h; 3 microspheres was increased at 24 h; 4+ microspheres was increased at 8 and 24 h (relative to the 0-h time point). For the NH_3 (+40 mV) surface type, two-way ANOVA indicates main effects of microspheres per cell ($F_{3,47} = 40$, $p < 0.0001$) and time ($F_{5,47} = 57$, $p < 0.0001$), and a significant interaction ($F_{15,\ 47} = 3.3$, $p = 0.0008$). Separate post hoc analyses (Dunnett's test) for each peak indicate that the percentage of cells containing 1 microsphere was increased at 4, 8, 24 h; 2 microspheres was increased at 4, 8, 24 h; 3 microspheres was increased at 4, 8, 24 h; 4+ microspheres was increased at 4, 8, 24 h (relative to the 0-h time point). Our data indicate that the OH (−70 mV) and COOH (−70 mV) microspheres may be internalized sequentially. Indeed, nearly all microsphere-containing cells had only one microsphere at 1 and 2 h, and then the percentage of cells with multiple microspheres per cell gradually increased over time suggesting that cells take up one microsphere at a time. For the NH_2 (−30 mV) and NH_3 (+40 mV) microspheres, the percentage of cells with multiple microspheres per cell increased more rapidly than for the OH (−70 mV) and COOH (−70 mV) microspheres, suggesting that a different mechanism may be responsible for internalizing these microspheres.

We then assessed the effect of size by comparing 1-µm microspheres (NH_2, −30 mV) with 1.5-µm microspheres with (NH_2, −38 mV). It was not possible to manufacture microspheres of different sizes with closer surface charge values. We assumed that the 8 mV charge difference between these microspheres was negligible. We first examined the effect of microsphere concentration on uptake over the concentration range (0.2–200 µg/ml) (Fig. 6a). Two-way ANOVA indicates a main effect of Concentration ($F_{3.16} = 601$, $p < 0.0001$) but not Size ($F_{1,16} = 0.2$, $p = 0.64$), and a significant interaction ($F_{3,16} = 5.0$, $p = 0.013$). Separate post hoc analyses for each microsphere size indicate that incubating 2, 20, and 200 µg/ml concentrations of the 1.5-µm microspheres, but only 20 and 200 µg/ml concentrations of the 1-µm microspheres, significantly increased the percentage of cells containing microspheres relative to values from the

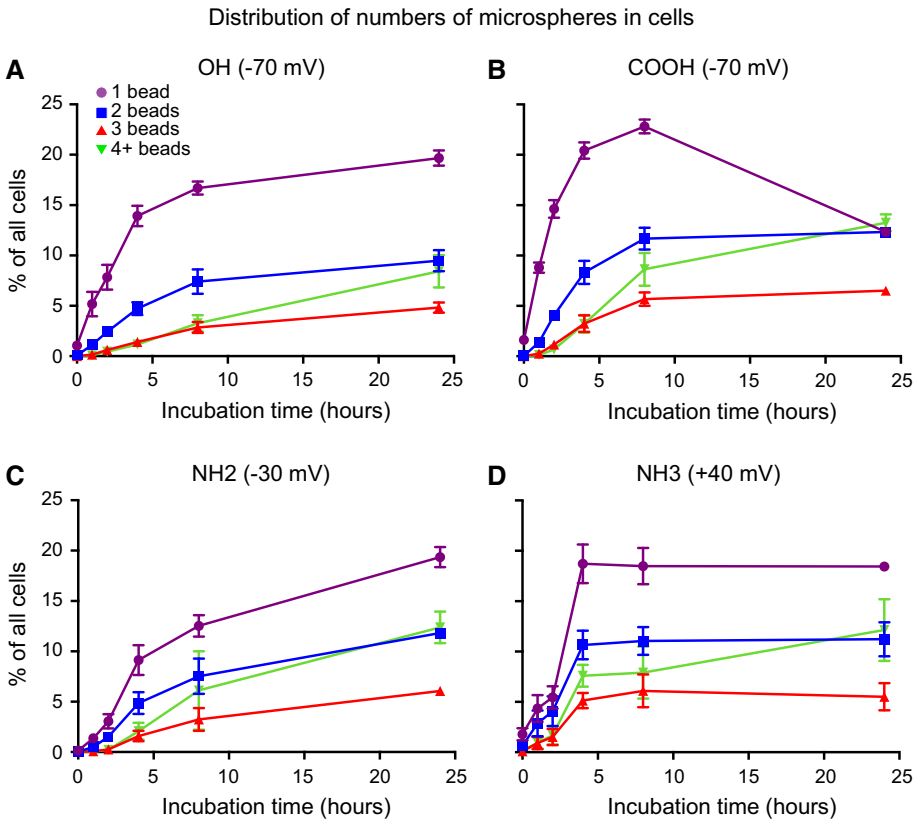

Fig. 5 Number of microspheres per cell. Data from the time course in Fig. 4b were re-analyzed to determine the percentage of live cells that contained 1, 2, 3, or 4+ microspheres. SH-SY5Y cells were incubated for 0–24 h with 5 µg/ml of the four different types of 1-µm microspheres. **a**, **b** For the OH (−70 mV) and COOH (−70 mV) microspheres, nearly all microsphere-containing cells had only one microsphere at 1–2 h, and then the percentage of cells with multiple microspheres per cell gradually increased over time. **c**, **d** For the NH_2 (−30 mV) and NH_3 (+40 mV) microspheres, the percentage of cells with multiple microspheres per cell increased more rapidly than for the OH (−70 mV) and COOH (−70 mV) microspheres. Data are shown as mean ± SEM, $n = 3$. Statistical analyses are shown in the "Results" section

0.2 μg/ml group. Overall, uptake of 1- and 1.5-μm microspheres was not significantly different from each other.

The percentage of cells with the 1- and 1.5-μm-size microspheres increased similarly with incubation time (Fig. 6b). Two-way ANOVA indicates a main effect of Time ($F_{5,24} = 56$, $p < 0.0001$), but not for Size ($F_{1,24} = 0.01$, $p = 0.90$) or interaction ($F_{5,24} = 1.3$, $p = 0.287$). Separate post hoc analyses (Dunnett's test) of each microsphere size indicate that 4, 8, and 24 h of incubation times significantly increased the percentage of cells containing microspheres, relative to values from the 0-h time point. Overall, uptake of 1- and 1.5-μm microspheres was not significantly different from each other.

We assessed microsphere uptake into primary cortical neurons (PCNs) obtained from P20 embryonic rat brains to better approximate the neurons in brain tissue (Fig. 7). Cells were incubated for either 4 or 8 h with 1-, 1.5-, or 2-μm microspheres (NH_2 chemistry with surface charges of −30, −38, and −22 mV respectively). Cell membranes were labeled with WGA conjugated to Alexa Fluor 647, while nuclei were labeled with DAPI. Deconvolution of confocal image z-stacks provided three orthogonal views (XY, XZ, YZ) of the red fluorescent microspheres inside the labeled cells. For all microsphere sizes, the microspheres were found within the cell membranes of all examined cells, which indicated that microspheres were internalized and not merely adsorbed to the outside of the cells.

Lastly, we assessed microsphere uptake into striatal cells of adult rats (Fig. 8). We injected 1-μm microspheres with NH_2 (−30 mV surface charge) directly into the striatum of live rats and assessed microsphere distribution 24 h later. The majority of microspheres did not diffuse far from the injection site. On average, microspheres diffused a radial distance of 387 μm outside the perimeter of the injection site, while maximal microsphere diffusion was 950 μm from the injection site. When microspheres diffused beyond the injection site, they were associated with sparsely distributed cells containing DAPI-labeled nuclei (Fig. 8a). PE fluorescent microspheres were associated with both neurons, as identified by Neurotrace membrane labeling (Fig. 8a, green), and unlabeled non-neuronal cells. Deconvolution of higher magnification confocal image stacks provided three orthogonal views (XY, XZ, YZ) of the red fluorescent microspheres inside the cell membranes of Neurotrace-labeled neurons (example shown in Fig. 8b).

Discussion

We used a combination of flow cytometry, epifluorescence, confocal, and electron microscopy to demonstrate that neurons in cell culture and in rat brain can internalize particles on the micron scale. Neuron-like SH-SY5Y neuroblastoma cells internalized microspheres with different surface types and charges (−70 to +40 mV), and sizes (1- and 1.5-μm) at approximately similar rates. Confocal and electron microscopy confirm that 1-, 1.5-, and even 2-μm microspheres were all internalized with no evidence of cell death compared to controls. Further support for internalization of microspheres in the flow cytometry assays is that the washing and trypsinization step to lift the SH-SY5Y cells from the plates should also have removed microspheres that were absorbed to the extracellular surface of these cells. Confocal microscopy indicated that post-

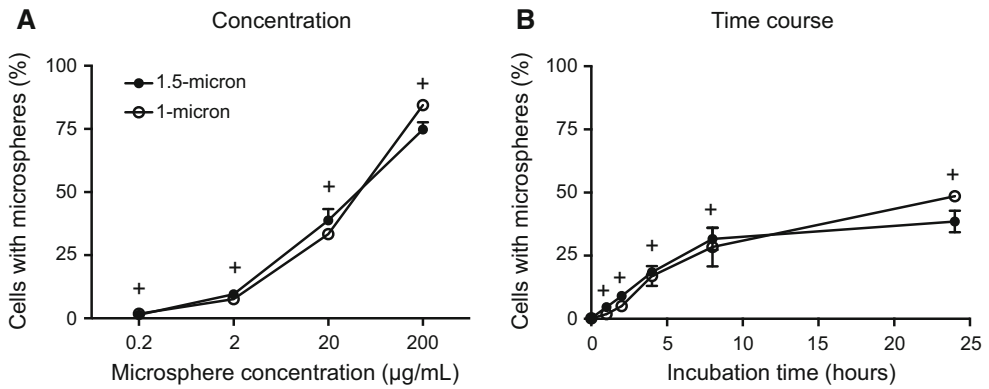

Fig. 6 Concentration and time course for internalization of 1- and 1.5-μm microspheres into SH-SY5Y cells. **a** SH-SY5Y cells were incubated for 3 h with 0.2–200 μg/ml of 1-μm NH_2 (−30 mV) or 1.5-μm NH_2 (−38 mV) microspheres and microsphere internalization was assessed using flow cytometry. Higher microsphere concentrations led to similar increases in the percentages of cells containing each size of microsphere. Data are shown as mean ± SEM, $n = 3$, *plus symbol* indicates significantly different from 0.2 μg/ml for each size of microsphere. **b** SH-SY5Y cells were incubated for 0–24 h with 5 μg/ml of 1-μm (–30 mV) or 1.5-μm NH_2 (–38 mV) microspheres. The cells rapidly internalized both sizes of microspheres within the first 8 h of incubation. Data are shown as mean ± SEM, $n = 3$, *plus symbol* indicates significantly different from 0-h time point for both sizes

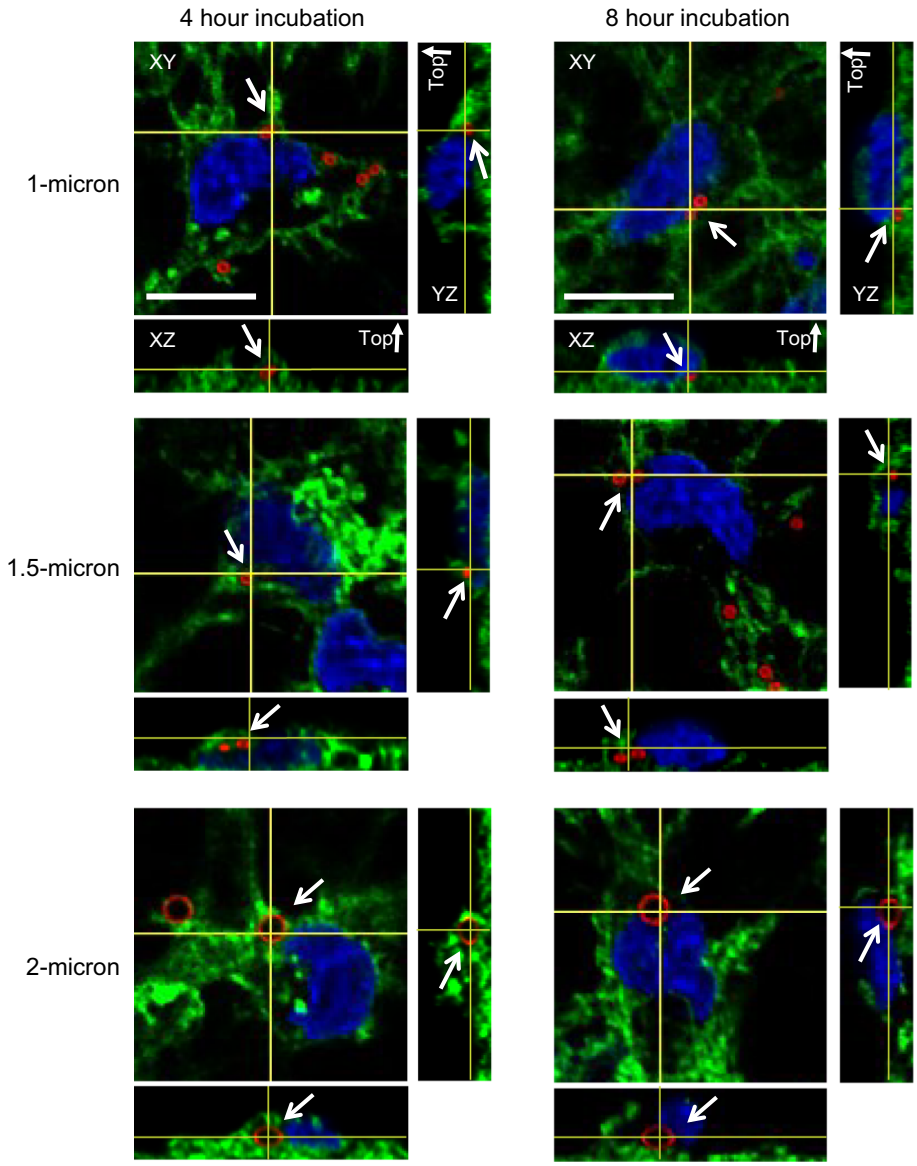

Fig. 7 Primary cortical neurons internalize 1, 1.5, and 2-μm microspheres. Primary cortical neurons were incubated for 4 or 8 h with 5 μg/ml of 1-, 1.5-, and 2-μm NH_2-functionalized microspheres (*red*) with surface charges of −30, −38, and −22 mV, respectively. After incubation, cell membranes were labeled with WGA-AF647 (*green*) and nuclei labeled with DAPI (*blue*). Following z-stack analysis of confocal microscope images, orthogonal views of the YZ and XZ planes indicate that the red fluorescent 1-, 1.5-, and 2-μm microspheres were internalized within the cell membrane. *White arrows* indicate red fluorescent microspheres. The '*Top*' label indicates the upper surface of the cells, furthest from the slide surface. *Scale bars* indicate 10 μm (Color figure online)

mitotic rat primary cortical neurons internalize 1-, 1.5-, and 2-μm microspheres. Confocal microscopy also indicated that at least 1-μm-size microspheres were internalized by neurons and other cell types following intracranial injections of the microspheres directly into striatum of adult rat brains, although distribution of the injected microspheres was not widespread. These data support the possibility of using intracellular micron-sized devices or delivery platforms in neurons for a variety of biotechnological applications.

Particle size is one factor that can affect particle internalization into cells (Frohlich et al. 2012; Rejman et al. 2004). Neurons in particular have historically been classified as non-phagocytic (Rabinovitch 1995), although there is little evidence to support this classification. Indeed, two previous studies indicate that neurons may internalize micron-scale particles by a phagocytotic mechanism (Ateh et al. 2011; Bowen et al. 2007). Our data indicate that neurons have the capacity to internalize particles up to 2 μm in diameter, well beyond the assumed endocytic size threshold of 0.5 μm of a non-phagocytic cell type (Rabinovitch 1995). At least for SH-SY5Y cells, uptake of 1 and 1.5 μm microspheres were equivalent over different concentrations and incubation times. The weight of evidence from the confocal and electron microscopy experiments supports internalization of particles into SH-SY5Y cells. However, it should be noted that separately (1) the quantitative assessment of microspheres associated with cells in the epifluorescence microscopy experiment may include some microspheres adsorbed (and not internalized) to cells while (2) we did not perform a quantitative assessment of the electron microscopy images to determine the exact ratio

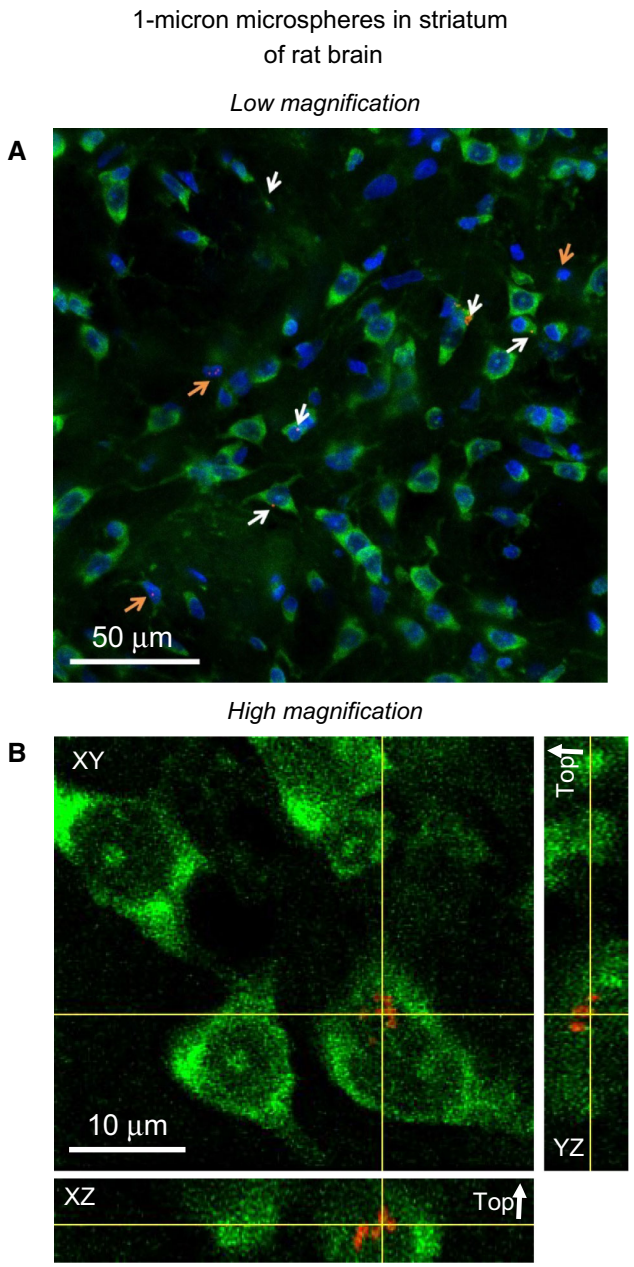

Fig. 8 Neurons in rat dorsal striatum internalize 1-µm microspheres. Adult rats were injected with 500 µg/ml 1-µm NH_2-functionalized microspheres with surface charge −30 mV in 1× PBS into striatum and perfused with 4% PFA 24 h later. **a** Low magnification (20× objective) maximum intensity projection image shows distribution and number of cells associated with red microspheres outside the injection site. Cell membranes of neurons only were labeled green with the fluorescent Nissl stain Neurotrace while nuclei were labeled blue with DAPI. White arrows indicate neurons with a microsphere while orange arrows indicate non-neuronal (unlabeled) cells with a microsphere. *Scale bar* indicates 50 µm. **b** Higher magnification (60× objective with 1.5 zoom) image to demonstrate internalization of microspheres into a sample neuron. Following z-stack analysis of confocal microscope images, orthogonal views of the YZ and XZ planes indicate that red fluorescent microspheres were internalized within the cell membrane. The *Top* label indicates the upper surface of the cells, furthest from the slide surface. *Scale bars* indicate 10 µm

of microspheres that were internalized versus those that were observed outside the cells. Primary cortical neurons in culture also internalized 1-, 1.5-, and 2-µm microspheres, and neurons in brain internalized 1-µm microspheres, although some of the microsphere-containing cells in our PCN cultures and certainly some of the microsphere-containing cells in the brain were not neurons.

Previous studies have focused on uptake of nano-sized particles into cells, and the effects of surface chemistry and charge on internalization are highly varied. While charge is thought to be a highly influential factor in determining particle internalization, little consensus has been achieved to determine whether positive, negative, or neutral charge facilitates or hinders particle internalization (Ayala et al. 2013; Bahmani et al. 2011; Harush-Frenkel et al. 2007; He et al. 2010; Kim et al. 2014; Wilhelm et al. 2003). Part of the difficulty in reaching consensus is the lack of consistency among testing conditions for various studies: chemistry of bead production, cell culture conditions, and in vivo techniques are highly variable and can yield vastly different results for any given particle and cell type. In the rat brain, we found microspheres in both Neurotrace-labeled neurons and Neurotrace-negative non-neuronal cells. We had not directly assessed the cell types of the non-neuronal cells in our striatal sections. However, based on previous literature, the striatum contains approximately equal numbers of neurons and non-neuronal cells (Gokce et al. 2016; Guez-Barber et al. 2012; Rubio et al. 2016). These non-neuronal cells comprise microglia, macrophages astrocytes, oligodendrocytes, ependymal cells, vascular cells, and stem cells. The microglia are well-documented phagocytic cells in the brain (Sole-Domenech et al. 2016) that may have internalized some of the microspheres in our rat brain experiment. We had not identified the different cell types in our PCN cultures. However, we had assessed the cell types in PCN cultures harvested and maintained in the same manner as in the current study (unpublished data from author Brandon Harvey) and found that the majority of cells are neurons (∼80% NeuN-positive cells), while the minority of cells are non-neuronal: ∼10–15% GFAP-labeled astrocytes, ∼5–10% nestin-labeled neural progenitor cells, <0.5% Iba1- or cd11b-labeled microglia, and <0.5% MBP-labeled oligodendrocytes.

Previous studies have also shown that different cell types respond differently to variably charged and functionalized particles (Gaiser et al. 2012; Georgieva et al. 2011; He et al. 2010). Our data suggest that neuronal cells can internalize a range of micron-sized particles over a range of surface charges and chemistry. Microsphere internalization varied with functional group and charge that also depended on incubation time and concentration. When microsphere concentration was increased, positively

charged microspheres associated more readily with neuronal cells compared to negatively charged microspheres. However, over the 24-h incubation period, positively charged ammonio-functionalized microspheres at +40 mV demonstrated a comparable rate of association with cells as −70 mV carboxyl-functionalized microspheres at a set concentration. These data highlight the importance of establishing controlled culture conditions when comparing microspheres of different charges and chemical groups.

Very little evidence exists for how neurons internalize microparticles larger than 0.5 μm. Other cell types known to possess phagocytic properties, such as macrophages, use complex, and diverse pathways even within the same cell types (Aderem 2003). Receptor binding and signal transduction can provide specificity for the mode of internalization and ultimate intracellular fate of extracellular material (Groves et al. 2008; Tollis et al. 2010), but overall the literature investigating these pathways is relatively limited (Freeman and Grinstein 2014). The mechanisms for phagocytosis in neurons, in particular, have not been investigated. Bowen et al. (2007) suggested that neurons may have limited immunological capacity that allows them to internalize micron-sized particles via pathways similar to that of phagocytes. The results from our confocal and electron microscopy suggest that neuronal cells may respond to micron-sized material in the environment and engulf material into the cytoplasm. However, electron microscopy indicated that the microspheres appeared cytosolic and did not localize within lysosomes or any other identifiable cell structure, as one would presume for entry via traditional phagocytic mechanisms. It is also possible that microspheres of the same size but different charge and functional group may be gaining entry to cells in different ways. Furthermore, the pathways of entry for micro-scale particles may be distinct from those used by nano-scale particles, and the mechanisms responsible for allowing microspheres to enter neuronal cells may be distinct from other cell types. Future studies will be necessary to elucidate the precise mechanisms of uptake in neurons.

Overall our data confirm and extend previous observations (Ateh et al. 2011; Bowen et al. 2007) that neurons in culture and in adult rodent brain can internalize particles in the micron range, and that their internalization can be affected by surface chemistry and charge. The mechanism of internalization is unknown but could be due to a receptor signaling pathway for non-specific material engulfment. The use of microparticles in brain has some obvious problems to solve in future studies. Following intracranial injections directly into brain, we observed poor distribution of 1-μm particles from the injection site. However, once neurons encountered microparticles, our results indicate that these neurons were able to internalize the microparticles. Given the range of charged and functionalized microspheres that we have shown to enter neurons, it appears likely that one can modify these microparticles to enhance their distribution in brain without altering neuronal uptake, and permit future neuroengineering and biomedical applications. Future studies are also necessary to identify the different types of non-neuronal cells in brain and in cell culture that internalized microspheres.

Acknowledgements This research was supported by the National Institute on Drug Abuse Intramural Research Program, NIH. Barbara Smith at the Johns Hopkins University Microscopy Core provided the electron microscopy services. The Johns Hopkins FACS Core facility was supported by the National Institute of Arthritis and Musculoskeletal and Skin Diseases of the National Institute of Health under Award Number P30AR053503.

References

Aderem A (2003) Phagocytosis and the inflammatory response. J Infect Dis 187(Suppl 2):S340–S345

Aderem A, Underhill DM (1999) Mechanisms of phagocytosis in macrophages. Annu Rev Immunol 17:593–623

Ateh DD, Leinster VH, Lambert SR, Shah A, Khan A, Walklin HJ, Johnstone JV, Ibrahim NI, Kadam MM, Malik Z, Girones M, Veldhuis GJ, Warnes G, Marino S, McNeish IA, Martin JE (2011) The intracellular uptake of CD95 modified paclitaxel-loaded poly(lactic-co-glycolic acid) microparticles. Biomaterials 32:8538–8547

Avdoshina V, Taraballi F, Dedoni S, Corbo C, Paige M, Saygideger Kont Y, Uren A, Tasciotti E, Mocchetti I (2016) Identification of a binding site of the human immunodeficiency virus envelope protein gp120 to neuronal-specific tubulin. J Neurochem 137:287–298

Ayala V, Herrera AP, Latorre-Esteves M, Torres-Lugo M, Rinaldi C (2013) Effect of surface charge on the colloidal stability and in vitro uptake of carboxymethyl dextran-coated iron oxide nanoparticles. J Nanopart Res 15:1874

Bahmani B, Gupta S, Upadhyayula S, Vullev VI, Anvari B (2011) Effect of polyethylene glycol coatings on uptake of indocyanine green loaded nanocapsules by human spleen macrophages in vitro. J Biomed Opt 16:051303

Benoit JP, Faisant N, Venier-Julienne MC, Menei P (2000) Development of microspheres for neurological disorders: from basics to clinical applications. J Control Release 65:285–296

Bowen S, Ateh DD, Deinhardt K, Bird MM, Price KM, Baker CS, Robson JC, Swash M, Shamsuddin W, Kawar S, El-Tawil T, Roos J, Hoyle A, Nickols CD, Knowles CH, Pullen AH, Luthert PJ, Weller RO, Hafezparast M, Franklin RJ, Revesz T, King RH, Berninghausen O, Fisher EM, Schiavo G, Martin JE (2007) The phagocytic capacity of neurones. Eur J Neurosci 25:2947–2955

Caron E, Hall A (1998) Identification of two distinct mechanisms of phagocytosis controlled by different Rho GTPases. Science 282:1717–1721

Chirra HD, Desai TA (2012) Multi-reservoir bioadhesive microdevices for independent rate-controlled delivery of multiple drugs. Small 8:3839–3846

Cleland JL (1999) Single-administration vaccines: controlled-release technology to mimic repeated immunizations. Trends Biotechnol 17:25–29

Doherty GJ, McMahon HT (2009) Mechanisms of endocytosis. Annu Rev Biochem 78:857–902

Ebert SN, Taylor DG, Nguyen HL, Kodack DP, Beyers RJ, Xu Y, Yang Z, French BA (2007) Noninvasive tracking of cardiac embryonic stem cells in vivo using magnetic resonance imaging techniques. Stem Cells 25:2936–2944

Freeman SA, Grinstein S (2014) Phagocytosis: receptors, signal integration, and the cytoskeleton. Immunol Rev 262:193–215

Frohlich E, Meindl C, Roblegg E, Ebner B, Absenger M, Pieber TR (2012) Action of polystyrene nanoparticles of different sizes on lysosomal function and integrity. Part Fibre Toxicol 9:26

Gaiser BK, Fernandes TF, Jepson MA, Lead JR, Tyler CR, Baalousha M, Biswas A, Britton GJ, Cole PA, Johnston BD, Ju-Nam Y, Rosenkranz P, Scown TM, Stone V (2012) Interspecies comparisons on the uptake and toxicity of silver and cerium dioxide nanoparticles. Environ Toxicol Chem 31:144–154

Georgieva JV, Kalicharan D, Couraud PO, Romero IA, Weksler B, Hoekstra D, Zuhorn IS (2011) Surface characteristics of nanoparticles determine their intracellular fate in and processing by human blood-brain barrier endothelial cells in vitro. Mol Ther 19:318–325

Gokce O, Stanley GM, Treutlein B, Neff NF, Camp JG, Malenka RC, Rothwell PE, Fuccillo MV, Sudhof TC, Quake SR (2016) Cellular taxonomy of the mouse striatum as revealed by single-cell RNA-seq. Cell Rep 16:1126–1137

Gordon S (2016) Phagocytosis: an immunobiologic process. Immunity 44:463–475

Groves E, Dart AE, Covarelli V, Caron E (2008) Molecular mechanisms of phagocytic uptake in mammalian cells. Cell Mol Life Sci 65:1957–1976

Guerrero-Cazares H, Tzeng SY, Young NP, Abutaleb AO, Quinones-Hinojosa A, Green JJ (2014) Biodegradable polymeric nanoparticles show high efficacy and specificity at DNA delivery to human glioblastoma in vitro and in vivo. ACS Nano 8:5141–5153

Guez-Barber D, Fanous S, Harvey BK, Zhang Y, Lehrmann E, Becker KG, Picciotto MR, Hope BT (2012) FACS purification of immunolabeled cell types from adult rat brain. J Neurosci Methods 203:10–18

Harush-Frenkel O, Debotton N, Benita S, Altschuler Y (2007) Targeting of nanoparticles to the clathrin-mediated endocytic pathway. Biochem Biophys Res Commun 353:26–32

He C, Hu Y, Yin L, Tang C, Yin C (2010) Effects of particle size and surface charge on cellular uptake and biodistribution of polymeric nanoparticles. Biomaterials 31:3657–3666

Henderson MJ, Richie CT, Airavaara M, Wang Y, Harvey BK (2013) Mesencephalic astrocyte-derived neurotrophic factor (MANF) secretion and cell surface binding are modulated by KDEL receptors. J Biol Chem 288:4209–4225

Howard DB, Powers K, Wang Y, Harvey BK (2008) Tropism and toxicity of adeno-associated viral vector serotypes 1, 2, 5, 6, 7, 8, and 9 in rat neurons and glia in vitro. Virology 372:24–34

Kaluzova M, Bouras A, Machaidze R, Hadjipanayis CG (2015) Targeted therapy of glioblastoma stem-like cells and tumor non-stem cells using cetuximab-conjugated iron-oxide nanoparticles. Oncotarget 6:8788–8806

Kim JE, Kim H, An SS, Maeng EH, Kim MK, Song YJ (2014) In vitro cytotoxicity of SiO_2 or ZnO nanoparticles with different sizes and surface charges on U373MG human glioblastoma cells. Int J Nanomedicine 9(Suppl 2):235–241

Lew DP, Andersson T, Hed J, Di Virgilio F, Pozzan T, Stendahl O (1985) Ca2+ -dependent and Ca2+ -independent phagocytosis in human neutrophils. Nature 315:509–511

Mukherjee S, Ghosh RN, Maxfield FR (1997) Endocytosis. Physiol Rev 77:759–803

Nakatsuji H, Numata T, Morone N, Kaneko S, Mori Y, Imahori H, Murakami T (2015) Thermosensitive ion channel activation in single neuronal cells by using surface-engineered plasmonic nanoparticles. Angew Chem Int Ed Engl 54:11725–11729

Pilakka-Kanthikeel S, Atluri VS, Sagar V, Saxena SK, Nair M (2013) Targeted brain derived neurotropic factors (BDNF) delivery across the blood-brain barrier for neuro-protection using magnetic nano carriers: an in vitro study. PLoS ONE 8:e62241

Rabinovitch M (1995) Professional and non-professional phagocytes: an introduction. Trends Cell Biol 5:85–87

Rejman J, Oberle V, Zuhorn IS, Hoekstra D (2004) Size-dependent internalization of particles via the pathways of clathrin- and caveolae-mediated endocytosis. Biochem J 377:159–169

Robinson JT, Jorgolli M, Shalek AK, Yoon MH, Gertner RS, Park H (2012) Vertical nanowire electrode arrays as a scalable platform for intracellular interfacing to neuronal circuits. Nat Nanotechnol 7:180–184

Rubio FJ, Li X, Liu QR, Cimbro R, Hope BT (2016) Fluorescence activated cell sorting (FACS) and gene expression analysis of Fos-expressing neurons from fresh and frozen rat brain tissue. J Vis Exp 114:e54358–e54358

Sahay G, Alakhova DY, Kabanov AV (2010) Endocytosis of nanomedicines. J Control Release 145:182–195

Sharpe MA, Marcano DC, Berlin JM, Widmayer MA, Baskin DS, Tour JM (2012) Antibody-targeted nanovectors for the treatment of brain cancers. ACS Nano 6:3114–3120

Simon DT, Gabrielsson EO, Tybrandt K, Berggren M (2016) Organic bioelectronics: bridging the signaling gap between biology and technology. Chem Rev 116:13009–13041

Skop NB, Calderon F, Levison SW, Gandhi CD, Cho CH (2013) Heparin crosslinked chitosan microspheres for the delivery of neural stem cells and growth factors for central nervous system repair. Acta Biomater 9:6834–6843

Sole-Domenech S, Cruz DL, Capetillo-Zarate E, Maxfield FR (2016) The endocytic pathway in microglia during health, aging and Alzheimer's disease. Ageing Res Rev 32:89–103

Stukel J, Thompson S, Simon L, Willits R (2015) Polyethlyene glycol microgels to deliver bioactive nerve growth factor. J Biomed Mater Res A 103:604–613

Taylor A, Herrmann A, Moss D, See V, Davies K, Williams SR, Murray P (2014) Assessing the efficacy of nano- and micro-sized magnetic particles as contrast agents for MRI cell tracking. PLoS ONE 9:e100259

Tollis S, Dart AE, Tzircotis G, Endres RG (2010) The zipper mechanism in phagocytosis: energetic requirements and variability in phagocytic cup shape. BMC Syst Biol 4:149

Varde NK, Pack DW (2004) Microspheres for controlled release drug delivery. Expert Opin Biol Ther 4:35–51

Vitale F, Summerson SR, Aazhang B, Kemere C, Pasquali M (2015) Neural stimulation and recording with bidirectional, soft carbon nanotube fiber microelectrodes. ACS Nano 9:4465–4474

Wang M, Alberti K, Sun S, Arellano CL, Xu Q (2014) Combinatorially designed lipid-like nanoparticles for intracellular delivery of cytotoxic protein for cancer therapy. Angew Chem Int Ed Engl 53:2893–2898

Wilhelm C, Billotey C, Roger J, Pons JN, Bacri JC, Gazeau F (2003) Intracellular uptake of anionic superparamagnetic nanoparticles as a function of their surface coating. Biomaterials 24:1001–1011

Yan L, Zhang J, Lee CS, Chen X (2014) Micro- and nanotechnologies for intracellular delivery. Small 10:4487–4504